Remote Sens. **2010**, *2*, 1177-1196; doi:10.3390/rs2041177

OPEN ACCESS

Remote Sensing

ISSN 2072-4292

www.mdpi.com/journal/remotesensing

Article

Potential of Using Remote Sensing Techniques for Global Assessment of Water Footprint of Crops

Mireia Romaguera [1,2,*], Arjen Y. Hoekstra [1], Zhongbo Su [2], Maarten S. Krol [1] and Mhd. Suhyb Salama [2]

[1] Faculty of Engineering Technology, Department of Water Engineering and Management, University of Twente, NL-7500 AE Enschede, The Netherlands; E-Mails: a.y.hoekstra@utwente.nl (A.H.); m.s.krol@utwente.nl (M.K.)

[2] Faculty of Geo-Information Science and Earth Observation, Department of Water Resources, University of Twente, NL-7500 AA Enschede, The Netherlands; E-Mails: b_su@itc.nl (Z.S.); salama@itc.nl (M.S.)

***** Author to whom correspondence should be addressed; E-Mail: romaguera@itc.nl.

Received: 10 February 2010; in revised form: 20 April 2010 / Accepted: 21 April 2010 / Published: 26 April 2010

Abstract: Remote sensing has long been a useful tool in global applications, since it provides physically-based, worldwide, and consistent spatial information. This paper discusses the potential of using these techniques in the research field of water management, particularly for 'Water Footprint' (WF) studies. The WF of a crop is defined as the volume of water consumed for its production, where green and blue WF stand for rain and irrigation water usage, respectively. In this paper evapotranspiration, precipitation, water storage, runoff and land use are identified as key variables to potentially be estimated by remote sensing and used for WF assessment. A mass water balance is proposed to calculate the volume of irrigation applied, and green and blue WF are obtained from the green and blue evapotranspiration components. The source of remote sensing data is described and a simplified example is included, which uses evapotranspiration estimates from the geostationary satellite Meteosat 9 and precipitation estimates obtained with the Climatic Prediction Center Morphing Technique (CMORPH). The combination of data in this approach brings several limitations with respect to discrepancies in spatial and temporal resolution and data availability, which are discussed in detail. This work provides new tools for global WF assessment and represents an innovative approach to global irrigation mapping, enabling the estimation of green and blue water use.

Keywords: water footprint; remote sensing; global scale; irrigation

1. Introduction

Accurate assessment of water use is an important issue in a globally changing climate and environment, where water is becoming a scarce but essential resource. In this context, the concept 'Water Footprint' (WF) was introduced by Hoekstra [1], and later elaborated on by Hoekstra and Chapagain [2], as an indicator that relates human consumption to global water resources. The WF of a crop is defined as the volume of water consumed for its production, where green and blue WF stand for rain and irrigation water usage, respectively. The importance of this parameter lies in the fact that international trade in commodities creates flows of what has been called 'virtual water' [3-5], by importing and exporting goods that require water. The indicator provides valuable information for a global assessment of how water resources are used. The WF can be calculated for goods, services, a specific activity, a business, an organization, an individual or for a community.

Remote sensing has long been a useful tool in global climate studies and hydrology, since it provides physically-based, worldwide, consistent spatial information [6-14], which represents a major improvement compared to the traditional point measurements. In the last few decades, the advances in science and technology have led to an increasing series of remotely sensed systems for Earth observation and monitoring, with applications in various fields of the environmental sciences, such as agriculture, meteorology, geology, land cover dynamics, global climate studies and hydrology. Nowadays, geostationary and polar-orbiting Earth observation satellites ensure global, multitemporal and multispectral coverage of the planet.

The aim of this paper is to discuss the potential of these techniques in the research field of water management, and in particular water footprint studies. Existing methods have calculated the WF and virtual water using data from national statistics, reports and climatic databases [4,15-17]. However, the use of remote sensing data has not yet been exploited in this field. The spatial and temporal coverage obtained with remote sensing data form an improvement over traditional *in situ* measurements. The spatial resolution is also improved, especially compared with data based on statistics or interpolated climatic station measurements, thus facilitating monitoring of the spatial variability of parameters.

In this paper, the potential use of remote sensing and its analysis techniques is illustrated to improve the understanding and estimation of a WF. An innovative remote sensing approach is presented for irrigation mapping, which enables the estimation of green and blue water use. However, global assessment of water footprints is outside the scope of this paper and will be considered during follow up research. The paper is organized in the following sections: In Section 2, the state of the art in WF estimations is described and how remote sensing data may improve final retrievals. The state of the art in global irrigation mapping is also incorporated in this section. A method for WF estimation is proposed in Section 3, where remote sensing estimates of precipitation, evapotranspiration, runoff, water storage and land use are employed. The data sources needed for this method are described in detail in this section and a simplified example is included. Finally, the approach and its limitations are discussed in Section 4.

2. State of the Art

2.1. Water Footprint of Crops

In recent years WFs and virtual water have been calculated for crops, goods, services, as well as on generic national levels [2,4,15-18].

The WF of crops forms the basis for WF estimations of crop products and derived commodities. The WF of a product is defined as the total volume of fresh water used to produce the product, summed over the various steps in the production chain [19].

Blue WF stands for irrigation water usage and green WF for rain water usage. In the case of irrigation, a part of the water withdrawn from the surface or groundwater system is evaporated between the point of withdrawal and the field, another part infiltrates and returns to the water source (and can be reused), and the rest reaches the field; there is a part that turns into drainage flow, which may be available for reuse as well. The blue WF refers to the sum of evaporation from storage reservoirs, transport canals and evapotranspiration from the field, although many previous studies have focused on the physical processes that happen in the field.

The main inputs for green and blue WF estimation are shown in Figure 1 and include crop evapotranspiration, area and volume of irrigation, water storage, runoff, crop characteristics, climatic data and crop production data.

Figure 1. Inputs for water footprint estimation.

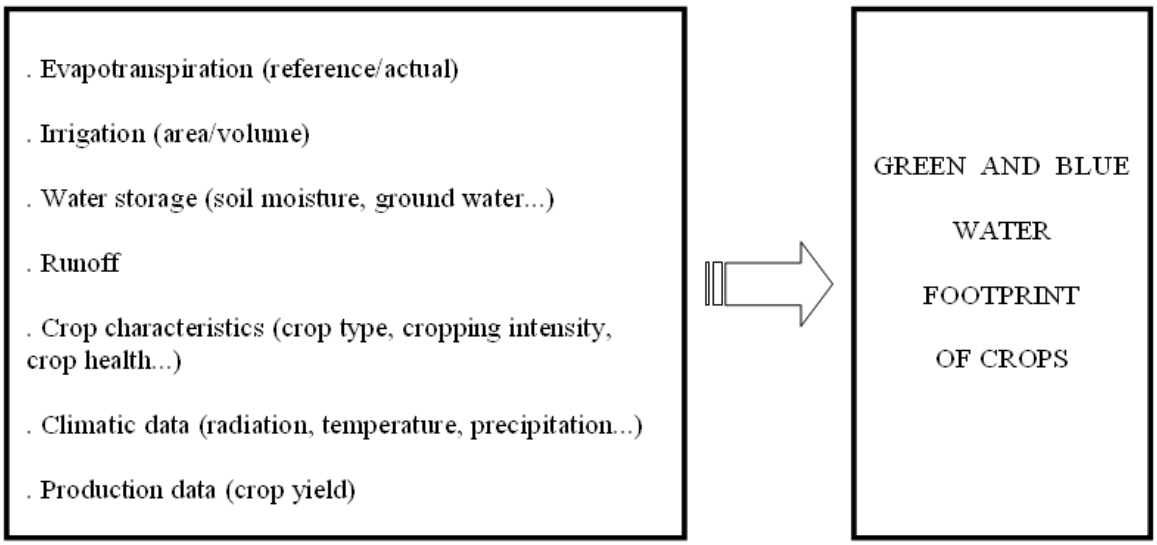

Hoekstra and Hung [4] carried out a global study to calculate the WF of crops based on crop yields and crop water requirements, where the latter were estimated following Allen *et al.* [20]. The results were presented per country and referred to the period 1995–1999. They made use of the CropWat model [21,22] of the Food and Agriculture Organization (FAO), with crop coefficient K_c, to estimate crop evapotranspiration. Crop yields were obtained from the FAOSTAT database [23]. Climatic data were taken from FAO's climatic database ClimWat [24], and crop parameters from the CropWat package. This model assumes that crops are planted under optimal soil moisture conditions, are disease-free, well-fertilized, grown in large fields with 100% coverage and have a single cropping pattern.

Siebert and Döll [17] provided blue and green virtual water content in global crop production. The results are presented at a spatial resolution of 5 arc minutes (approximately 10 km at the equator), for 26 different crops, and refer to the period 1998–2002. Their Global Crop Water model (GCWM) is based on a soil water balance where actual evapotranspiration is calculated according to Allen *et al.* [20] using the crop and stress coefficients (K_c and K_s), and irrigation at time *(t+1)* is computed by subtracting the actual available soil water at time *t* from the total soil water capacity. This model uses the cropping pattern and cropping season information of Portmann *et al.* [25] as input, as well as climate data derived from the Climate Research Unit (CRU) of the University of East Anglia dataset [26] and crop coefficients according to Allen *et al.* [20].

Liu *et al.* [15] estimated blue and green water components of consumptive water use for a range of agricultural crops with a spatial resolution of 30 arc minutes (approximately 55 km at the equator) for the period 1998–2002. Their model simulated crop yield, total evapotranspiration and crop water productivity [27]. The data sets used in this study included maps of harvested areas by Ramankutty *et al.* [28] and Portmann *et al.* [29]. Climatic data were obtained from the CRU dataset [26], crop fertilizer application from statistical reports and soil parameters from work by Batjes [30].

Mekonnen and Hoekstra [16] estimated the global blue and green WF of wheat with a resolution of 5 arc minutes (approximately 10 km at the equator) for the period 1996–2005. In this approach, actual evapotranspiration and irrigation requirements were calculated according to Allen *et al.* [20] using crop and stress coefficients (K_c and K_s). The total WF at each grid cell was estimated to be the weighted average of the WFs in a rainfed and an irrigated scenario. Weighting was based on the actual presence of irrigation. The method also derived yield data and the grey WF, which is defined as the volume of freshwater required to assimilate the load of pollutants, based on existing ambient water quality [19]. This work used reference evapotranspiration data from FAO [24], precipitation data from CRU [26], irrigated area values from national and AQUASTAT databases [31] as well as from Portmann *et al.* [29], and the Global Map of Irrigation Areas (GMIA) from Siebert *et al.* [32].

All the aforementioned approaches are based on the concept of evapotranspiration with the objective of estimating blue and/or green water use. However, the input used, and the type of output produced, differ. The results are presented at different spatial resolutions, namely country scale, 5, and 30 arc minutes. Different data sources are considered in the methods, such as national statistics, reports, climatic databases and crop-related maps, with different spatial and temporal resolutions. In some cases, the crops are assumed to be growing in ideal conditions, *i.e.,* their irrigation requirement is met and growing characteristics are optimal. In addition, the results presented cover different time periods. This leads to the following limitations:

1. coarse spatial resolution of the source data, mainly where extracted from statistical databases,
2. coarse temporal resolution of the input data, which may imply the use of interpolation techniques,
3. assumption of ideal conditions, e.g., optimum soil water conditions,
4. outputs are static, *i.e.*, they are given for particular periods of time.

On the other hand, remote sensing techniques provide global coverage, varied temporal and spatial resolution and broad spectral information, countering these limitations. Monitoring crops in an appropriate space and time scale may, as a result, provide better estimates of blue and green water use.

In particular, five aspects have been identified which may be estimated and show improvement with the use of remote sensing techniques on a global scale: retrieval of actual evapotranspiration, quantification of precipitation, mapping of land use, estimation of surface runoff, and quantification of water storage. In addition, this paper proposes an innovative method for quantifying the amount of irrigation, using the aforementioned parameters. In order to have an overview of existing methods, the next section discusses the state of the art in global irrigation mapping.

2.2. Irrigation Mapping

In recent years, several studies have approached the problem of global irrigation mapping, using national statistical data as input [32,33] or making use of spectral and temporal remote sensing data for classification [34,35].

Siebert *et al.* [32,33] provided a global map of areas equipped for irrigation (GMIA) with a spatial resolution of 5 arc minutes, around the year 2000. The input in this approach consisted of data from FAO reports, the United Nations, the World Bank, Ministries of Agriculture, irrigation associations, printed maps, digital datasets and the land cover data set of the United States Geological Survey (USGS) for the year 2000. This method combined sub-national statistical data with land cover information to produce output at a grid resolution. The results are given in terms of percentage of surface area equipped for irrigation. The quality of the map is assessed by taking into account the density of the statistical information available and the amount of agreement between different data sources. The map is also compared with global land cover datasets, revealing large discrepancies.

Thenkabail *et al.* [35] developed the Global Irrigated Area Map (GIAM) with 28 classes and a spatial resolution of 10 km, around year 1999. Temporal series of remote sensing data were used in this work. Reflectance values, brightness temperatures and Normalized Difference Vegetation Index (NDVI) were obtained from the Advanced Very High Resolution Radiometer (AVHRR). NDVI estimates were acquired at a higher resolution from the Système Pour l'Observation de la Terre Vegetation (SPOT VGT) and precipitation data were obtained from the Japanese Earth Resources Satellite-1 Synthetic Aperture Radar (JERS-1 SAR). A digital elevation model and a global tree cover map were used as input as well. The method is based on classification and identification techniques to establish different classes of irrigated areas and to differentiate irrigated areas from non-irrigated areas. Global ground-truth data from approximately 5,600 locations and Landsat Enhanced Tematic Mapper Plus (ETM+) mosaics were used as training data for the classification. The 28 class global map provides classes labeled based on irrigation source (surface water, groundwater or conjunctive use), intensity (single, double or continuous crop) and crop dominance. The map shows discrepancies with the map of irrigated areas produced by Siebert *et al.* [33], and with national statistics from India. However, linear relations between the data are found with correlation coefficients of 0.94 and 0.76 (1:1 line), respectively.

Ozdogan and Gutman [34] used Moderate Resolution Imaging Spectroradiometer (MODIS) data to produce a 500 m resolution irrigation map for the United States. The input data for this approach were the Nadir Bidirectional Distribution Function Adjusted Reflectance (NBAR) data acquired during 2001. In this work, a climatic moisture index was calibrated to define irrigation potential. In addition, spectral indices such as the NDVI and the greenness index were identified. The method is based on a

supervised classification of the remotely sensed data and the irrigation potential. Ancillary data for training the model are Landsat images, climatic data, county based irrigated area maps, and state reports. The method provides a binary classification into irrigated and non-irrigated classes, and a fractional area estimate of each pixel identified as irrigated. The output is compared with sub-national statistics providing a rms error of 2% of the total irrigated area.

Regarding the type of inputs, the different methods obtain their data mainly from national statistics, or from remote sensing estimates such as NDVI, brightness temperatures and surface reflectance values. The methods are based on classification techniques applied to data time series.

Regarding output, the aforementioned methods provide information about areas equipped for irrigation, about crop dominance and irrigation source, and about existence or absence of irrigation. None of the methods quantify the actual amount of water received by the crops through irrigation, from here onwards called 'actual irrigation'.

The present paper proposes an innovative approach for the retrieval of actual irrigation on a global scale. First of all, as input, the method uses water cycle components such as evapotranspiration, precipitation, surface runoff and water storage from remote sensing techniques. Secondly, a physically-based method is applied, whereas previous studies applied classification techniques to the remote sensing data. Finally, making use of the temporal resolution of remote sensing data, this method will allow actual irrigation maps to be obtained on time scales of a month or a season, representing a physically more correct monitoring of the processes involved. This forms an improvement over existing methods, which provided static estimates for particular years only.

3. Methodology

3.1. Theory

The use of Earth Observation (EO) estimates of precipitation, evapotranspiration, surface runoff, and water storage is proposed to estimate actual irrigation. The mass water balance in an irrigated area A [L^2] for time period dt is given by:

$$P + I = ET + Q + \frac{dS}{dt} \tag{1}$$

where P [LT^{-1}] is precipitation, I [LT^{-1}] is actual irrigation, ET [LT^{-1}] is actual evapotranspiration, Q [LT^{-1}] is surface runoff/streamflow, and S [L] is water storage in a vertical column (snow, canopy water storage, soil moisture and groundwater). Therefore, the retrieval of I is ensured as soon as the other parameters are estimated.

In addition, for the analysis of green and blue water use, ET is divided into a green water component (ET_g), and a blue water component (ET_b):

$$ET = ET_g + ET_b \tag{2}$$

For regions with negligible runoff, ET_g and ET_b may be assumed to occur proportionally to the input from precipitation and irrigation, on a sufficiently long time scale. Other cases need to be analyzed with a more complex approach.

The green component in the water footprint of a crop (WF_g, m^3/ton) is calculated as the green component in crop water use (CWU_g, m^3/ha) divided by the crop yield (Y, ton/ha), according to Hoekstra *et al.* [19]. The blue component is calculated in a similar way:

$$WF_g = \frac{CWU_g}{Y}, \qquad WF_b = \frac{CWU_b}{Y} \tag{3}$$

The green and blue components in crop water use are calculated by accumulation of daily evapotranspiration (mm/day) over the total growing period:

$$CWU_g = 10 \cdot \sum_{d=1}^{lgp} (ET_g)_d, \qquad CWU_b = 10 \cdot \sum_{d=1}^{lgp} (ET_b)_d \tag{4}$$

where the factor 10 is meant to convert water depths in mm into water volumes per land surface in m^3/ha. Summation takes place from the day of planting (day 1) to the day of harvesting (lgp stands for length of the growing period in days).

Figure 2 shows the flowchart of the input needed and the output desired for WF estimations. The first step of the proposed methodology consists of using remote sensing estimates of P, ET, Q and S for retrieving I by means of equation (1) on a global scale. The separation of croplands from other land covers and the differentiation of crops are elicited from land use maps obtained with remote sensing. Next, ET_g and ET_b need to be modeled and obtained from ET, P and I. The calculation of the components of the WF per crop is carried out by using equations (3) and (4). Finally, crop yields are based on statistics.

Figure 2. Flowchart proposed for obtaining WF of crops from remote sensing data.

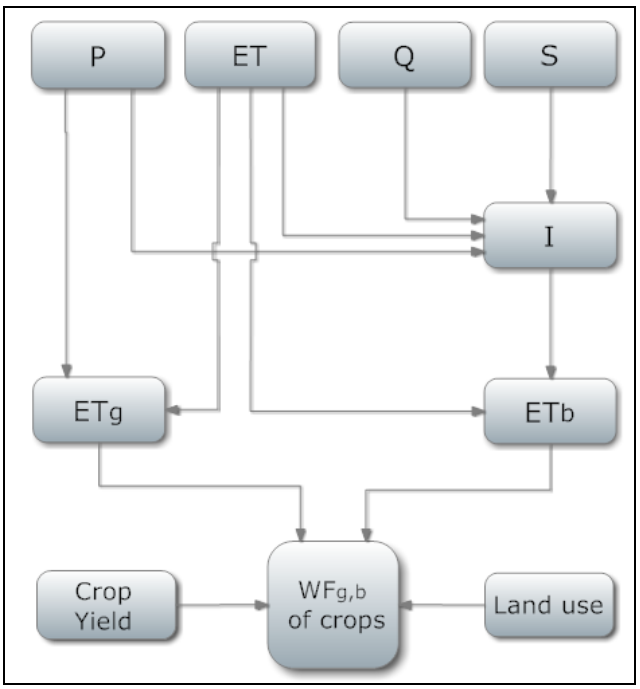

The data sources available on a global scale through remote sensing techniques are detailed in the next sections, as well as the methods employed for obtaining the different types of input.

3.2. Global EO Products

Table 1 shows an overview of the sources of data and available global EO products. The table also includes information on spatial coverage, spatial and temporal resolution, main inputs, and data availability.

Table 1. Earth observation products (incomplete) involved in Equation (1): Source, spatial coverage, spatial and temporal resolution, main inputs and availability of data.

EO product	Source	Spatial coverage	Spatial resolution	Temporal resolution	Main input	Data availability
P	CMORPH	Global	8 km at the equator	30’ monthly	MW IR	2002–present
	PERSIANN	Global	0.25 °	6h	IR	2000–present
	MPE	Meteosat disk *	Met7:5 km at nadir Met8:3 km at nadir Met9:3 km at nadir	Met7: 30’ Met8: 15’ Met9: 15’	MW IR	2000–present
ET	MET	Meteosat disk *	3 km at nadir	30’	Radiation fluxes LAI, FVC Climatic data	Pre-operational (available)
	MOD 16	Global	1 km	daily	Land cover LAI, FAPAR Climatic data	Pre-operational (not available)
S	GRACE	Global	400 km	monthly	Gravity fields	2002–present
Q	GLDAS	Global	1 °	3h monthly	Land cover LAI and soil par. Skin temperature Radiation fluxes Climatic data	1979–present

*Meteosat disk covers latitudes between −60 °and +60 °and longitudes between −60 °to +60 °.

**List of acronyms: CMORPH (Climate Prediction Center Morphing Technique), PERSIANN (Precipitation Estimation from Remotely Sensed Information using Artificial Neural Networks), MPE (Multisensor Precipitation Estimate), MET (Meteosat EvapoTranspiration), MOD 16 (MODIS product 16), GRACE (Gravity Recovery and Climate Experiment), GLDAS (Global Land Data Assimilation System).

EO data on global precipitation can be obtained from different sources, such as the Climatic Prediction Center (CPC) Morphing Technique (CMORPH), which produces global precipitation estimates every 30 minutes with a resolution of 8 km at the equator. This technique uses precipitation estimates that have been derived from low orbiting satellite microwave (MW) observations exclusively. Infrared (IR) information from geostationary satellites with a higher temporal resolution is used to retrieve cloud motion vectors. The precipitation values are then interpolated in time, based on the motion of the clouds [11]. Another source is the Precipitation Estimation from Remotely Sensed Information using Artificial Neural Networks (PERSIANN) system that uses neural network techniques to estimate rainfall rate at six hourly intervals for each $0.25° \times 0.25°$ pixel (approximately 30 km at the equator) of the infrared brightness temperature image provided by geostationary satellites [36,37].

At a continental scale, the Multisensor Precipitation Estimate (MPE) produces precipitation estimates from Meteosat 7, 8 and 9 satellites. The data from Meteosat 7 (Met7) are generated every 30 minutes with a spatial resolution of 5 km at nadir. Meteosat 8 (Met8) and Meteosat 9 (Met9) data have a temporal resolution of 15 minutes and a spatial resolution of 3 km at nadir. The method combines passive microwave data from the Special Sensor Microwave Imager (SSM/I) and images in the Meteosat IR channel [38].

Remote sensing evapotranspiration data (Meteosat EvapoTranspiration, MET) are available from the Land Surface Analysis-Satellite Applications Facility (LSA-SAF) at a temporal resolution of 30 minutes, for the disk of Meteosat Second Generation (MSG) satellites, and are in a pre-operational phase at present. The method is based on forcing a Soil-Vegetation-Atmosphere-Transfer (SVAT) scheme with relevant data (short and long-wave radiation fluxes, albedo, leaf area index (LAI), fraction of vegetation cover (FVC) and snow cover) derived from Meteosat and auxiliary data (air temperature, humidity, wind speed, atmospheric pressure, *etc*.) from other sources, mainly from the European Center for Medium-Range Weather Forecast (ECMWF) [39]. Other products on a global scale that are in pre-operational phase and not yet available at present are derived from MODIS on a daily basis at a 1 km resolution (MODIS product MOD 16). The algorithm for retrieving these products is based on the Penman-Monteith equation for computing evapotranspiration and uses MODIS land cover, Fraction of Photosynthetic Active Radiation Absorbed by the vegetation (FAPAR) and LAI, as well as global surface meteorology from the Global Modeling and Assimilation Office (GMAO) [12].

The change in water storage (the dS/dt term) includes water storage in the vertical column, *i.e.*, snow, canopy water storage, soil moisture and groundwater. Global data on water storage are obtained from the satellite GRACE (Gravity Recovery and Climate Experiment) at a resolution of 400 km on a monthly basis. The sensors measure temporal variations in the gravity field that can be used to estimate changes in terrestrial water storage [13,40]. The data are presented as equivalent height of water.

Finally, global data on runoff are provided by the Global Land Data Assimilation System (GLDAS) [41]. The system integrates different land surface models based on satellite and ground-based observational data. In particular, the Variable Infiltration Capacity (VIC) model focuses on runoff processes and uses an infiltration curve to characterize them [42]. These data are provided every three hours and on a monthly basis, with a spatial resolution of 1 ° (approximately 110 km at the equator).

3.3. Estimation of Evapotranspiration from Remote Sensing Data

At present, the possibility of obtaining operational ET data using remote sensing on a global scale is not widely available. Therefore, an overview of existing methods is included. Remote sensing techniques have meant an important improvement in actual evapotranspiration estimation, since they allow monitoring spatial and temporal variability beyond traditional point measurements. Many analyses have been carried out in the past decades using remote sensing data on a regional to global scale, and by applying empirical and/or physically-based methods. The one-dimensional methods, Surface Energy Balance System (SEBS) [43] and Two-source Energy Balance (TSEB) Model [44], are physically-based surface energy balance models. Other methods make use of the spatial variability of

the surface temperature and reflectance and/or vegetation index observations, such as the Surface Energy Balance (SEBAL) approach [45] and the Simplified Surface Energy Balance Index (S-SEBI) method [46]. Others use direct correlations between vegetation indices and evaporation [47]. Actual evapotranspiration can also be estimated using the FAO approach [20], which uses reference ET (e.g., from the Penman-Monteith method) combined with crop specific coefficients. All these approaches have been applied to sensors onboard different platforms, such as the Along-Track Scanning Radiometer (ATSR), the Advanced Spaceborne Thermal Emission and Reflection Radiometer (ASTER), AVHRR and Landsat [48-53]. On a global scale, the fusion of data from different sensors ensures full coverage. However, the parameters that are involved in this process should be observed at relevant scales.

3.4. Land Use from Remote Sensing Data

Different land cover maps are available on a global scale, such as the Global Land Cover 2000 Project (GLC 2000) [10] and the MODIS yearly global product for the period 2001–2004 [54], both at a 1 km resolution. The Medium Resolution Imaging Spectrometer (MERIS) GlobCover product for 2005 [55,56] is produced at a 300 m resolution. These maps are based on classification techniques and distinguish between generic land cover classes such as croplands, forests, desert areas, savannas, shrublands, *etc*. In order to identify different types of crops, several approaches have been proposed. For example, Zhang *et al.* [57] made use of Fast Fourier Transforms on MODIS NDVI series, Blaes *et al.* [58] discussed the synergy of optical and Synthetic Aperture Radar (SAR) image time series for this purpose and Rao [59] developed a spectral library from *in situ* hyperspectral data to carry out classification of a remote sensing image.

3.5. Example

This section provides a simplified example, where ET_g and ET_b are obtained for Egypt in October 2009. In this country, the contrast between the non irrigated desert areas and the irrigated croplands in the Nile basin is very clear.

The calculations were carried out for Equation (1) over a period of one month. In this case, there is no runoff due to the characteristics of study area: dry conditions with low monthly precipitation in October 2009 (less than 30 mm) and highly permeable soils. Furthermore, in this example, for simplicity reasons the storage term (dS/dt) is assumed to be negligible, meaning that all actual irrigation transforms into evapotranspiration. Therefore, actual irrigation is calculated according to:

$$\left.\begin{array}{l} P + I = ET + Q + \dfrac{dS}{dt} \\ Q = 0 \\ \dfrac{dS}{dt} = 0 \end{array}\right\} \rightarrow \quad I = ET - P \tag{5}$$

Precipitation data were obtained from the CPC Famine Early Warning System Network (FEWS-NET) data archive on a daily base and were aggregated to a monthly value. Pre-operational Meteosat-9 ET values were acquired from LSA-SAF with a temporal resolution of 30 minutes.

Instantaneous values of ET were integrated during the day and summed to a monthly value. Linear interpolation was used to fill in missing data. ET values were not considered if the lack of data occurred during a period of one hour or longer. In general terms, the percentage of day-time acquisitions used for the calculations was 97%.

The two components, ET_g and ET_b, were retrieved by assuming that they both occur as input in a proportional way (precipitation and irrigation). The results are shown in Figures 3a and 3b. The maps show the distinction between the croplands and vast desert areas where P and therefore ET are negligible. For the period of analysis, the evapotranspiration in the Egyptian croplands is mainly due to blue water contribution, especially in the Nile basin area with values up to 80 mm per month. The contribution of green water to the total ET is concentrated in the coastal regions, yielding values of up to 30 mm per month.

Figure 3. (a) Monthly green ET and (b) Monthly blue ET obtained in October 2009, using remote sensing data in Egypt.

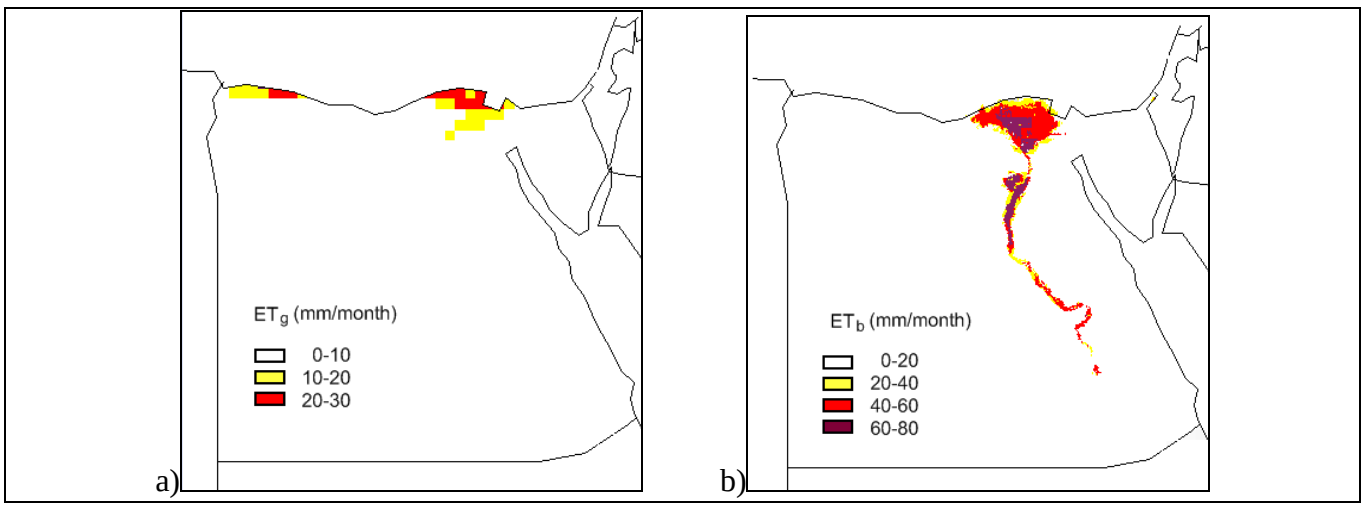

Extending these calculations over the entire crop growing period and combining them with data on crop yield and land use, following the approach of Hoekstra *et al.* [19], will eventually provide the WF for these crops (Equations (3) and (4)). As an illustration, Table 2 provides some existing blue and green WFs of wheat for different countries obtained for the period 1996–2005 by Mekonnen and Hoekstra [16]. These countries have the largest blue water footprints of wheat, accounting for 88% of the total blue WF related to wheat production. Aggregated WF values for all Egypt have a value of 47,330 Mm^3/year obtained for the period 1997–2001 in Hoekstra and Chapagain [2].

Table 2. Blue and green water footprint of wheat in India, China, Pakistan, Iran, Egypt, United States and total in the world obtained for the period 1996–2005 (from Mekonnen and Hoekstra [16]).

Country	Blue WF (Mm^3/year)	Green WF (Mm^3/year)
India	81,335	44,025
China	47,370	83,459
Pakistan	27,733	12,083
Iran	10,940	26,699
Egypt	5,930	1,410
United States	5,503	111,926
World	203,744	760,301

4. Discussion

4.1. Uncertainty

In this paper, the use of remote sensing estimates is proposed for mapping actual irrigation, using Equation (1), where inaccuracies will propagate and combine in the underlying data. The contribution of the different parameters to the total error in I is assessed by means of a sensitivity analysis using the first order Taylor series expansion, where the covariance terms have been neglected and linearity has been assumed:

$$\sigma(I)=\sqrt{\left(\frac{\partial I}{\partial P}\right)^2\cdot\sigma^2(P)+\left(\frac{\partial I}{\partial ET}\right)^2\cdot\sigma^2(ET)+\left(\frac{\partial I}{\partial Q}\right)^2\cdot\sigma^2(Q)+2\cdot\left(\frac{\partial I}{\partial S}\right)^2\cdot\sigma^2(S)}= \\ =\sqrt{\sigma^2(P)+\sigma^2(ET)+\sigma^2(Q)+2\cdot\sigma^2(S)} \quad (6)$$

where σ(I) is the standard deviation in the error of retrieving I, $\partial/\partial x$ represent the partial derivatives with respect to x, with x denoting a factor influencing I, and σ(P), σ(ET), σ(Q), σ(S) are the standard deviations associated to the errors in estimating P, ET, Q and S. The change in storage (dS/dt) is calculated as the subtraction of two estimates of S, therefore a factor of 2 is added in the sensitivity analysis.

The components of the uncertainty given in Equation (6) are determined through prior knowledge of the range of their actual values. CMORPH precipitation estimates are highly dependent on the rainfall regime [60,61], with biases of ±10% during the cold season and between 50% and 175% during the warm season [62]. Kalma *et al.* [63] showed that remote sensing data provided relative errors of 15–30% in evapotranspiration estimation. The storage term obtained from GRACE contains validation errors, in terms of 'equivalent water height', of 2–3 cm, according to Liu *et al.* [64]. Finally, runoff estimates are highly dependent on the land surface model used in GLDAS, where validation activities provided annual differences lower than 30% in the basins of Europe by using the VIC model [65]. In this analysis, three values for monthly precipitation (50, 100 and 200 mm), and errors of 10% and 100% are considered. Three scenarios of ET are analyzed with values of 0, 5 and 10 mm/day and a value of 2.5 cm is assumed for the accuracy of the storage term. An average value of 100 mm/month and an error of 15% are considered for the runoff.

The advantage of using Equation (6) is that the relative contribution of each error component to the total error level in the irrigation map can be easily computed. The analysis of the relative errors shows that in the case of a low precipitation error, the inaccuracy in I is mainly determined by the storage term, with values between 58 and 83%, increasing with the precipitation value. When a higher precipitation error is considered, the precipitation term contributes to the total error for between 59 and 95%. In all cases, the influence of ET and runoff errors is lower than 15%. This means that the error in irrigation estimation is mainly influenced by the accuracy of the estimates for precipitation and water storage, and shows the necessity for improving the accuracy of precipitation and water storage figures derived from remote sensing data, as also reported by Sheffield *et al.* [66]. Alternatively, integration into the model of other data sources, such as higher resolution remote sensing estimates or ground data, may potentially improve the accuracy of the retrievals. Finally, the uncertainty in water footprint estimation will obviously also depend on model structure and on inaccuracies in crop classification and yield.

4.2. Limitations

This paper proposes the use of EO estimates for mapping actual irrigation on a global scale. However, the combination of the different inputs provides limitations, since the data differ in terms of spatial coverage, spatial and temporal resolution and availability.

Global coverage will only be ensured when global evapotranspiration products become available or alternatively when derived from global remote sensing data as described in Section 3.3. Moreover, calculation of ET is partly hampered by clouds, since they are opaque to visible and infrared radiation from the surface, which form the main input for ET estimation. Modeling techniques, such as the work by Farah [67], are needed to cover these intermediate periods. Special attention has to be paid to this phenomenon in tropical latitudes. Global ET products are foreseen from MODIS based on the Penman-Monteith equation [12] and from MSG satellites by applying a two-source model covering Europe, Africa and Mideast [68].

Moreover, the combination of multi-resolution data implies the use of specific fusion algorithms. Additional techniques are needed when multi-spectral data are combined, for example when retrieving ET with existing methods. An overview of these fusion techniques is provided in Dong *et al.* [69].

The estimates also differ in terms of temporal resolution. This heterogeneity can be solved by aggregating the data to time steps of one month or a season.

Regarding the availability of data, the lack of operative global ET products constitutes one of the main limitations. In the near future, Meteosat 8 and 9 ET data will be operational, thus achieving coverage for Europe and Africa. Other global ET products foreseen are mentioned above and may alternatively be derived from existing remote sensing techniques. The availability of the remaining data in Table 1 ensures WF calculations from the year 2002 onwards.

With respect to historical data, the ECMWF ReAnalysis (ERA 40 and ERA Interim [70,71]) provides meteorological data since 1979. Precipitation and runoff are obtained by assimilating different types of data, among them remote sensing information. GLDAS [41] has been providing runoff estimates and water storage components, such as snow, soil moisture and canopy storage, since 1979. The land surface models of GLDAS partly incorporate remotely sensed data. Groundwater

historical data may be obtained from national and regional administrations, although in a limited temporal and spatial resolution. Alternatively, groundwater may be modeled by using hydrological approaches [72,73]. Evapotranspiration may be derived from historical data sets like 'Pathfinder AVHRR/8 km land (PAL)' [74], which are available in terms of brightness temperature and top of the atmosphere reflectance for the years 1981–1999.

Furthermore, the combination of parameters obtained from different sources with different methods may lead to consistency problems. For example, precipitation is used in two steps of the calculations. Firstly it is obtained from MW and IR observations in CMORPH. Secondly, precipitation is an input in GLDAS, which is used to estimate runoff. The precipitation in GLDAS is obtained from the US Naval Research Laboratory (NRL) and the Goddard Space Flight Center (GSFC) products, whereas CMORPH estimates are calculated independently. This may lead to methodological differences and therefore special attention must be paid to the consistency of these estimates.

Different data sets are available for estimating the WF as shown in Table 1. Of these sets, CMORPH precipitation and MODIS ET products have the highest spatial resolution while providing global coverage. GRACE data have the advantage of accounting for groundwater from a remote sensing point of view, but have a coarse resolution (400 km). With respect to runoff, consistency of the estimates needs to be assessed as discussed in the example above. Furthermore, runoff must be investigated jointly with precipitation and irrigation in order to properly subdivide ET into blue and green components.

Recognizing the use of GRACE data constitutes a limitation in this model in terms of spatial resolution, leading to several issues. Firstly, the gravity field based observation techniques are continuously improved, as was shown with the launch in March 2009 of the Gravity field and steady-state Ocean Circulation Explorer (GOCE), which achieves a spatial resolution finer than 100 km. Secondly, GRACE estimates may be combined with soil moisture remote sensing products at a higher resolution, such as the Special Sensor Microwave/Imager (SSM/I) estimates with a spatial resolution of 70 by 45 km and available since early 90s. Finally, data assimilation may also be considered in the model in order to support the remote sensing data with ground truth observations. This will bring the necessity of harmonization of data, in terms of pixel resampling and calibration, and spatial modeling, so that the data are merged and analyzed in a data information system.

In general, downscaling techniques may be used to increase the resolution of remote sensing data. However, the debate is ongoing in defining the spatial resolution needed for observing the processes, while at the same time preserving feasibility for application with global coverage. For example, ground water and precipitation could be analyzed at lower resolution than evapotranspiration or soil moisture, since the processes occur at a higher scale and they present a lower spatial variability. Therefore, relevant scales should be defined, and in some cases the relation between remote sensing input and the processes that occur in the field will be difficult to observe.

5. Conclusions

This paper describes the potential of using remote sensing techniques for global water footprint estimation. The parameters involved in the proposed method are precipitation, evapotranspiration, water storage, surface runoff and land use. These parameters may be acquired from available global

products or alternatively may be derived with existing methods. A mass water balance is proposed to calculate the volume of irrigation applied, and green and blue WF are obtained from the green and blue evapotranspiration components. The combination of data in this approach brings several limitations with respect to discrepancies in spatial and temporal resolution and data availability. At present, the major limitation is the lack of operative global ET products to be obtained through remote sensing. Furthermore, the coarse spatial resolution of the water storage term obtained with GRACE, may be improved by using techniques of data assimilation and downscaling. Regarding the accuracy of the approach, the sensitivity analysis shows the necessity for improving the accuracy of precipitation and water storage figures derived from remote sensing data. Moreover, the separation of ET into de blue and green components requires a more elaborate modeling for accounting for the diversity of scenarios. In general terms, WF calculations using remote sensing can only be carried out over recent years (2002–present). However, ancillary data taken from alternative sources may be used, such as meteorological data from ECMWF, or land surface models that run with reanalysis data, together with remote sensing databases such as the Pathfinder database. This will ensure time coverage from the year 1979 onwards.

Acknowledgement

The authors wish to thank the referees and the guest editor of the special issue, Prasad Thenkabail, for their constructive remarks which have assisted us to improve the quality of the manuscript.

References

1. Hoekstra, A.Y. Virtual water trade. In *Proceedings of the International Expert Meeting on Virtual Water Trade*; Value of Water Research Report Series No.12, IHE Delft, The Netherlands, 2003.
2. Hoekstra, A.Y.; Chapagain, A.K. *Globalization of Water. Sharing the Planet's Freshwater Resources*; Blackwell Publishing: Oxford, UK, 2008; pp. 1-208.
3. Allan, J.A. Virtual water: A strategic resource global solutions to regional deficits. *Ground Water* **1998**, *36*, 545-546.
4. Hoekstra, A.Y.; Hung, P.Q. Globalisation of water resources: international virtual water flows in relation to crop trade. *Global Environ. Change* **2005**, *15*, 45-56.
5. Chapagain, A.K.; Hoekstra, A.Y. The global component of freshwater demand and supply: an assessment of virtual water flows between nations as a result of trade in agricultural and industrial products. *Water Int.* **2008**, *33*, 19-32.
6. Baret, F.; Hagolle, O.; Geiger, B.; Bicheron, P.; Miras, B.; Huc, M.; Berthelot, B.; Nino, F.; Weiss, M.; Samain, O.; Roujean, J.L.; Leroy, M. LAI, fAPAR and fCover CYCLOPES global products derived from VEGETATION—Part 1: Principles of the algorithm. *Remote Sens. Environ.* **2007**, *110*, 275-286.
7. Wagner, W.; Scipal, K. Large-scale soil moisture mapping in western Africa using the ERS scatterometer. *IEEE Trans. Geosci. Remote Sens.* **2000**, *38*, 1777-1782.
8. Sobrino, J.A.; Romaguera, M. Land surface temperature retrieval from MSG1-SEVIRI data. *Remote Sens. Environ.* **2004**, *92*, 247-254.

9. Guanter, L.; Gomez-Chova, L.; Moreno, J. Coupled retrieval of aerosol optical thickness, columnar water vapor and surface reflectance maps from ENVISAT/MERIS data over land. *Remote Sens. Environ.* **2008**, *112*, 2898-2913.
10. Bartholome, E.; Belward, A.S. GLC2000: A new approach to global land cover mapping from Earth observation data. *Int. J. Remote Sens.* **2005**, *26*, 1959-1977.
11. Joyce, R.J.; Janowiak, J.E.; Arkin, P.A.; Xie, P.P. CMORPH: A method that produces global precipitation estimates from passive microwave and infrared data at high spatial and temporal resolution. *J. Hydrometeorol.* **2004**, *5*, 487-503.
12. Mu, Q.; Heinsch, F.A.; Zhao, M.; Running, S.W. Development of a global evapotranspiration algorithm based on MODIS and global meteorology data. *Remote Sens. Environ.* **2007**, *111*, 519-536.
13. Rodell, M.; Velicogna, I.; Famiglietti, J.S. Satellite-based estimates of groundwater depletion in India. *Nature* **2009**, *460*, 999-U980.
14. Melesse, A.M.; Shih, S.F. Spatially distributed storm runoff depth estimation using Landsat images and GIS. *Comput. Electron. Agric.* **2002**, *37*, 173-183.
15. Liu, J.G.; Zehnder, A.J.B.; Yang, H. Global consumptive water use for crop production: The importance of green water and virtual water. *Water Resour. Res.* **2009**, *45*, 15.
16. Mekonnen, M.M.; Hoekstra, A.Y. *A Global and High-Resolution Assessment of the Green, Blue and Grey Water Footprint of Wheat*; Value of Water Research Report No.42; UNESCO-IHE: Delft, The Netherlands, 2010.
17. Siebert, S.; Döll, P. Quantifying blue and green virtual water contents in global crop production as well as potential production losses without irrigation. *J. Hydrol.* **2010**, *384*, 198-217.
18. Hoekstra, A.Y.; Chapagain, A.K. Water footprints of nations: Water use by people as a function of their consumption pattern. *Water Resour. Manag.* **2007**, *21*, 35-48.
19. Hoekstra, A.Y.; Chapagain, A.K.; Aldaya, M.M.; Mekonnen, M.M. *Water Footprint Manual. State of the Art 2009*; Water footprint Network: Enschede, The Netherlands, 2009.
20. Allen, R.; Pereira, L.S.; Raes, D.; Smith, M. *FAO Irrigation and Drainage Paper No. 56: Crop Evapotranspiration*; FAO in UN: Rome, Italy, 1998.
21. Smith, M. *CROPWAT:Manual and Guidelines*; FAO in UN: Rome, Italy, 1991.
22. FAO. *CROPWAT 8.0 Model*; Food and Agriculture Organization: Rome, Italy, Available online: www.fao.org/nr/water/infores_databases_cropwat.html (accessed on 22 April 2010).
23. FAO. *FAOSTAT Database*; Food and Agriculture Organization: Rome, Italy, Available online: http://faostat.fao.org (accessed on 22 April 2010).
24. FAO. *CLIMWAT 2.0 Database*; Food and Agriculture Organization: Rome, Italy, Available online: www.fao.org/nr/water/infores_databases_climwat.html (accessed on 22 April 2010).
25. Portmann, F.T.; Siebert, S.; Döll, P. MIRCA2000-Global Monthly Irrigated and Rainfed Crop Areas around the year 2000: A new high-resolution data set for agricultural and hydrological modeling. *Glob. Biogeochem. Cycle* **2010**, doi:10.1029/2008GB003435; (in press).
26. Mitchell, T.D.; Jones, P.D. An improved method of constructing a database of monthly climate observations and associated high-resolution grids. *Int. J. Climatol.* **2005**, *25*, 693-712.
27. Liu, J.; Wiberg, D.; Zehnder, A.J.B.; Yang, H. Modeling the role of irrigation in winter wheat yield, crop water productivity, and production in China. *Irrig. Sci.* **2007**, *26*, 21-33.

28. Ramankutty, N.; Evan, A.T.; Monfreda, C.; Foley, J.A. Farming the planet: 1. Geographic distribution of global agricultural lands in the year 2000. *Glob. Biogeochem. Cycle* **2008**, *22*, doi:1010.1029/2007GB002952.
29. Portmann, F.; Siebert, S.; Bauer, C.; Döll, P. *Global Data Set of Monthly Growing Areas of 26 Irrigated Crops*; Institute of Physical Geography, University of Frankfurt (Main): Frankfurt , Germany, 2008.
30. Batjes, N.H. *ISRIC-WISE Derived Soil Properties on a 5 by 5 Arc-Minutes Global Grid*; International Soil Reference & Information Centre: Wageningen, The Netherlands, 2006.
31. FAO. *AQUASTAT Database*; Food and Agriculture Organization: Rome, Italy, Available online: www.fao.org/nr/water/aquastat/main/index.stm (accessed on 22 April 2010).
32. Siebert, S.; Hoogeveen, J.; Frenken, K. *Irrigation in Africa, Europe and Latin America. Update of the Digital Global Map of Irrigation Areas to Version 4*; Institute of Physical Geography, University of Frankfurt (Main): Frankfurt, Germany, 2006.
33. Siebert, S.; Döll, P.; Hoogeveen, J.; Faures, J.M.; Frenken, K.; Feick, S. Development and validation of the global map of irrigation areas. *Hydrol. Earth Syst. Sci.* **2005**, *9*, 535-547.
34. Ozdogan, M.; Gutman, G. A new methodology to map irrigated areas using multi-temporal MODIS and ancillary data: An application example in the continental US. *Remote Sens. Environ.* **2008**, *112*, 3520-3537.
35. Thenkabail, P.S.; Biradar, C.M.; Noojipady, P.; Dheeravath, V.; Li, Y.J.; Velpuri, M.; Gumma, M.; Gangalakunta, O.R.P.; Turral, H.; Cai, X.L.; Vithanage, J.; Schull, M.A.; Dutta, R. Global irrigated area map (GIAM), derived from remote sensing, for the end of the last millennium. *Int. J. Remote Sens.* **2009**, *30*, 3679-3733.
36. Hsu, K.L.; Gao, X.G.; Sorooshian, S.; Gupta, H.V. Precipitation estimation from remotely sensed information using artificial neural networks. *J. Appl. Meteorol.* **1997**, *36*, 1176-1190.
37. Hsu, K.-l.; Gupta, H.V.; Gao, X.; Sorooshian, S. Estimation of physical variables from multichannel remotely sensed imagery using a neural network: Application to rainfall estimation. *Water Resour. Res.* **1999**, *35*, 1605-1618.
38. Heinemann, T.; Latanzio, A.; Roveda, F. The Eumetsat multi-sensor precipitation estimate (MPE). In *Second International Precipitation Working group (IPWG) Meeting*, Madrid, Spain, September 2002.
39. Gellens-Meulenberghs, F.; Arboleda, A.; Ghilain, N. Towards a continuous monitoring of evapotranspiration based on MSG data. In *Proceedings of Symposium HS3007 at IUGG2007*, Perugia, Italy, July 2007; IAHS Publication 316, IAHS Press: Oxfordshire, UK, 2007; pp. 228.
40. Swenson, S.; Wahr, J. Monitoring the water balance of Lake Victoria, East Africa, from space. *J. Hydrol.* **2009**, *370*, 163-176.
41. Rodell, M.; Houser, P.R.; Jambor, U.; Gottschalck, J.; Mitchell, K.; Meng, C.J.; Arsenault, K.; Cosgrove, B.; Radakovich, J.; Bosilovich, M.; Entin, J.K.; Walker, J.P.; Lohmann, D.; Toll, D. The global land data assimilation system. *Bull. Amer. Meteorol. Soc.* **2004**, *85*, 381-394.
42. Nijssen, B.; Schnur, R.; Lettenmaier, D.P. Global retrospective estimation of soil moisture using the variable infiltration capacity land surface model, 1980–93. *J. Clim.* **2001**, *14*, 1790-1808.
43. Su, Z. The Surface Energy Balance System (SEBS) for estimation of turbulent heat fluxes. *Hydrol. Earth Syst. Sci.* **2002**, *6*, 85-99.

44. Norman, J.M.; Kustas, W.P.; Humes, K.S. Source approach for estimating soil and vegetation energy fluxes in observations of directional radiometric surface temperature. *Agric. For. Meteorol.* **1995**, *77*, 263-293.
45. Bastiaanssen, W.G.M.; Menenti, M.; Feddes, R.A.; Holtslag, A.A.M. A remote sensing surface energy balance algorithm for land (SEBAL)—1. Formulation. *J. Hydrol.* **1998**, *213*, 198-212.
46. Roerink, G.J.; Su, Z.; Menenti, M. S-SEBI: A simple remote sensing algorithm to estimate the surface energy balance. *Phys. Chem. Earth P B-Hydrol. Oceans Atmos.* **2000**, *25*, 147-157.
47. Glenn, E.P.; Huete, A.R.; Nagler, P.L.; Hirschboeck, K.K.; Brown, P. Integrating remote sensing and ground methods to estimate evapotranspiration. *Crit. Rev. Plant Sci.* **2007**, *26*, 139-168.
48. Anderson, M.C.; Norman, J.M.; Mecikalski, J.R.; Otkin, J.A.; Kustas, W.P. A climatological study of evapotranspiration and moisture stress across the continental United States based on thermal remote sensing: 1. Model formulation. *J. Geophys. Res.-Atmos.* **2007**, *112*, 17.
49. French, A.N.; Jacob, F.; Anderson, M.C.; Kustas, W.P.; Timmermans, W.; Gieske, A.; Su, Z.; Su, H.; McCabe, M.F.; Li, F.; Prueger, J.; Brunsell, N. Surface energy fluxes with the Advanced Spaceborne Thermal Emission and Reflection radiometer (ASTER) at the Iowa 2002 SMACEX site (USA). *Remote Sens. Environ.* **2005**, *99*, 55-65.
50. Jia, L.; Su, Z.B.; van den Hurk, B.; Menenti, M.; Moene, A.; De Bruin, H.A.R.; Yrisarry, J.J.B.; Ibanez, M.; Cuesta, A. Estimation of sensible heat flux using the Surface Energy Balance System (SEBS) and ATSR measurements. *Phys. Chem. Earth* **2003**, *28*, 75-88.
51. van der Kwast, J.; Timmermans, W.; Gieske, A.; Su, Z.; Olioso, A.; Jia, L.; Elbers, J.; Karssenberg, D.; de Jong, S. Evaluation of the Surface Energy Balance System (SEBS) applied to ASTER imagery with flux-measurements at the SPARC 2004 site (Barrax, Spain). *Hydrol. Earth Syst. Sci.* **2009**, *13*, 1337-1347.
52. Sobrino, J.A.; Gomez, M.; Jimenez-Munoz, C.; Olioso, A. Application of a simple algorithm to estimate daily evapotranspiration from NOAA-AVHRR images for the Iberian Peninsula. *Remote Sens. Environ.* **2007**, *110*, 139-148.
53. Bastiaanssen, W.G.M.; Pelgrum, H.; Wang, J.; Ma, Y.; Moreno, J.F.; Roerink, G.J.; van der Wal, T. A remote sensing surface energy balance algorithm for land (SEBAL)—2. Validation. *J. Hydrol.* **1998**, *213*, 213-229.
54. Friedl, M.A.; McIver, D.K.; Hodges, J.C.F.; Zhang, X.Y.; Muchoney, D.; Strahler, A.H.; Woodcock, C.E.; Gopal, S.; Schneider, A.; Cooper, A.; Baccini, A.; Gao, F.; Schaaf, C. Global land cover mapping from MODIS: algorithms and early results. *Remote Sens. Environ.* **2002**, *83*, 287-302.
55. ESA *GLOBCOVER Products Description Manual v2*; European Space Agency: Paris, France, 2008.
56. Arino, O.; Gross, D.; Ranera, F.; Leroy, M.; Bicheron, P.; Brockman, C.; Defourny, P.; Vancutsem, C.; Achard, F.; Durieux, L.; Bourg, L.; Latham, J.; Di Gregorio, A.; Witt, R.; Herold, M.; Sambale, J.; Plummer, S., GlobCover: ESA service for Global Land Cover from MERIS. In *IGARSS 2007*, Barcelona, Spain, 2007; pp. 2412-2415.
57. Zhang, M.W.; Zhou, Q.B.; Chen, Z.X.; Liu, J.; Zhou, Y.; Cai, C.F. Crop discrimination in Northern China with double cropping systems using Fourier analysis of time-series MODIS data. *Int. J. Appl. Earth Obs. Geoinf.* **2008**, *10*, 476-485.

58. Blaes, X.; Vanhalle, L.; Defourny, P. Efficiency of crop identification based on optical and SAR image time series. *Remote Sens. Environ.* **2005**, *96*, 352-365.
59. Rao, N.R. Development of a crop-specific spectral library and discrimination of various agricultural crop varieties using hyperspectral imagery. *Int. J. Remote Sens.* **2008**, *29*, 131-144.
60. Ebert, E.E.; Janowiak, J.E.; Kidd, C. Comparison of near-real-time precipitation estimates from satellite observations and numerical models. *Bull. Amer. Meteorol. Soc.* **2007**, *88*, 47-64.
61. Tian, Y.; Peters-Lidard, C.D.; Choudhury, B.J.; Garcia, M. Multitemporal analysis of TRMM-based satellite precipitation products for land data assimilation applications. *J. Hydrometeorol.* **2007**, *8*, 1165-1183.
62. Sapiano, M.R.P.; Arkin, P.A. An intercomparison and validation of high-resolution satellite precipitation estimates with 3-Hourly gauge data. *J. Hydrometeorol.* **2009**, *10*, 149-166.
63. Kalma, J.D.; McVicar, T.R.; McCabe, M.F. Estimating land surface evaporation: A review of methods using remotely sensed surface temperature data. *Surv. Geophys.* **2008**, *29*, 421-469.
64. Liu, X.; Ditmar, P.; Siemes, C.; Slobbe, D.C.; Revtova, E.A.; Klees, R.; Riva, R.; Zhao, Q. DEOS Mass Transport model (DMT-1) based on GRACE satellite data: methodology and validation. *Geophys. J. Intl.* **2010**, doi: 10.1111/j.1365-246X.2010.04533.x.
65. Zaitchik, B.F.; Rodell, M.; Olivera, F. Evaluation of the Global Land Data Assimilation System using global river discharge data and a source to sink routing scheme. *Water Resour. Res.* **2010**, doi:10.1029/2009WR007811.
66. Sheffield, J.; Ferguson, C.R.; Troy, T.J.; Wood, E.F.; McCabe, M.F. Closing the terrestrial water budget from satellite remote sensing. *Geophys. Res. Lett.* **2009**, *36*, 5.
67. Farah, H.O. Estimation of Regional Evaporation under Different Weather Conditions from Satellite and Meteorological Data: A Case Study in the Naivasha basin, Kenya. Ph.D. Thesis; ITC Dissertation No. 80; University of Twente: Enschede, The Netherlands, 2001.
68. Anderson, M.C.; Norman, J.M.; Mecikalski, J.R.; Otkin, J.A.; Kustas, W.P. A climatological study of evapotranspiration and moisture stress across the continental United States based on thermal remote sensing: 2. Surface moisture climatology. *J. Geophys. Res.-Atmos.* **2007**, *112*, 13.
69. Dong, J.; Zhuang, D.F.; Huang, Y.H.; Fu, J.Y. Advances in multi-sensor data fusion: Algorithms and applications. *Sensors* **2009**, *9*, 7771-7784.
70. ECMWF. ERA-40: ECMWF 45-year reanalysis of the global atmosphere and surface conditions 1957–2002. ECMWF Newsletter 101; ECMWF: Reading, UK, 2004.
71. ECMWF. Towards a climate data assimilation system: Status update of ERA-Interim. ECMWF Newsletter 115; ECMWF: Reading, UK, 2008.
72. Barthel, R.; Sonneveld, B.; Gotzinger, J.; Keyzer, M.A.; Pande, S.; Printz, A.; Gaiser, T. Integrated assessment of groundwater resources in the Oueme basin, Benin, West Africa. *Phys. Chem. Earth* **2009**, *34*, 236-250.
73. Chatterjee, R.; Purohit, R.R. Estimation of replenishable groundwater resources of India and their status of utilization. *Curr. Sci.* **2009**, *96*, 1581-1591.

74. Agbu, P.A.; James, M.E. *The NOAA/NASA Pathfinder AVHRR Land Data Set User's Manual*; Goddard Distributed Active Archive Center, NASA, Goddard Space Flight Center: Greenbelt, MD, USA, 1994.